International Journal of Plasticity 105 (2018) 225–238

Contents lists available at ScienceDirect

International Journal of Plasticity

journal homepage: www.elsevier.com/locate/ijplas

Universally scaling Hall-Petch-like relationship in metallic glass matrix composites

Y.Y. Liu[a,b], P.Z. Liu[b], J.J. Li[a], P.K. Liaw[c], F. Spieckermann[d], D. Kiener[d], J.W. Qiao[a,b,*], J. Eckert[d,e]

[a] College of Materials Science and Engineering, Taiyuan University of Technology, Taiyuan, 030024, China
[b] Key Laboratory of Interface Science and Engineering in Advanced Materials, Ministry of Education, Taiyuan University of Technology, Taiyuan, 030024, China
[c] Department of Materials Science and Engineering, The University of Tennessee, Knoxville, TN, 37996-2200, USA
[d] Department Materials Physics, Montanuniversität Leoben, Jahnstraße 12, A-8700, Leoben, Austria
[e] Erich Schmid Institute of Materials Science, Austrian Academy of Sciences, Jahnstraße 12, A-8700, Leoben, Austria

ARTICLE INFO

Keywords:
Metallic glasses composites
Tension ductility
Work hardening
Hall-Petch-like relationship
Mean-field theory

ABSTRACT

Ti-based metallic glass matrix composites (MGMCs) with a composition of $Ti_{50}Zr_{20}V_{10}Cu_5Be_{15}$ (atomic percent, at. %) exhibit excellent tensile ductility and distinct work-hardening capability. A dislocation pile-up model (DPM) has been established to elaborate the dislocation motion near the yield point and to theoretically derive a linear Hall-Petch-like relationship between the yield strength, σ, and the inverse square root of the diameter of dendrite arms, $d^{-1/2}$. The materials constant, k, in the present Hall-Petch-like relationship can be calculated on the basis of the pile-up model, and is very close to the experimental value. The hardness variation in the dendrites and the strengthening effect from unloading-reloading tests prove the reasonability of the DPM during tension. The Hall-Petch-like relationship is verified for a variety of MGMCs, whose plastic deformation is only dominated by dislocation motion. Mean-field theory (MFT) has been first utilized to build a relationship between the critical diameter of dendrites, d_c, and the composition in MGMCs with the similar atomic percentages of low solubility elements. By tuning the composition, one can universally scale the Hall-Petch-like relationship, and accurately predict the yield strength of such in-situ MGMCs.

1. Introduction

Bulk metallic glasses (BMGs), compared with traditional crystalline alloys, are well-known for their unique mechanical properties, such as the high yield strength, large elastic limit, and high hardness, together with excellent corrosion and wear resistance, etc. (Hofmann, 2010; Schuh et al., 2007; Wang et al., 2004). Nevertheless, due to the rapid development of highly-localized shear bands upon loading at ambient temperature, BMGs usually exhibit poor ductility and fail catastrophically, which greatly restricts their applications as potential structural engineering materials (Chen and Dai, 2016; Eckert et al., 2011; Greer et al., 2013; Hufnagel et al., 2016). In order to retard rapid shear banding in BMGs and promote the generation of multiple shear bands, metallic glass matrix composites (MGMCs) reinforced by *in-situ* secondary dendritic phases have been successfully developed to enhance room-temperature plasticity effectively (Eckert et al., 2011; Hofmann et al., 2008a; Qiao et al., 2009a, 2016a). Recently, more and more studies on such dendrite-reinforced MGMCs mainly focus on the very composites with high specific strength and large tensile ductility

* Corresponding author. College of Materials Science and Engineering, Taiyuan University of Technology, Taiyuan 030024, China.
E-mail address: qiaojunwei@gmail.com (J.W. Qiao).

https://doi.org/10.1016/j.ijplas.2018.02.015
Received 28 October 2017; Received in revised form 22 February 2018; Accepted 23 February 2018
Available online 06 March 2018

(Hofmann et al., 2008b; Jiang et al., 2015a). Thereinto, Ti-based MGMCs have attracted much attention for their easy processing, excellent mechanical properties, low density, and high glass-forming ability of glass matrices, which may contribute to their dramatically-improved processing potential and lightweight applications (Fornell et al., 2009; Hofmann et al., 2008b; Jiang et al., 2015a; Qiao et al., 2012).

During the plastic deformation of such dual-phase Ti-based MGMCs, as the soft crystalline phases (dendrites) are embedded uniformly in the glass matrix, ductile dendrites can impede the quick shear-band propagation and promote the multiplication of shear bands. This trend can result in global tensile ductility at room temperature (Hofmann et al., 2008b; Jiang et al., 2015a; Qiao et al., 2011, 2012; Zhang et al., 2014). To further investigate the plastic-deformation mechanisms of such composites in more detail, together with a tremendous improvement in the tensile ductility, compared with monolithic BMGs, Qiao et al. (Qiao et al., 2011, 2013; Sun et al., 2015a) have proposed constitutive relationships, based on different deformation stages to elaborate the deformation mechanisms upon room-temperature tension. According to the stress-strain curves and the deformation modes of two phases, the tension behavior has been divided into three stages: (1) elastic (elastic-elastic and elastic-plastic), (2) work-hardening (plastic-plastic), and (3) softening (plastic-plastic) (Qiao et al., 2011; Sun et al., 2015a). Moreover, Zhang et al. (Jeon et al., 2016; Zhang et al., 2014) have proposed that the size of the dendrites plays a significant role for the tensile ductility of MGMCs, and the yield strength increases with decreasing the dendrite size. The effect of the volume fractions and sizes of dendrites on tension ductility have been widely studied (Hofmann et al., 2008b; Lee et al., 2004). However, the dependence of the yield strength on the dendrite size is yet to be studied quantitatively. Generally, in conventional polycrystalline alloys, the yield strength significantly increases with the decrease of the grain size, and the flow stress follows a Hall-Petch relationship (Meyers et al., 2006). Meanwhile, the materials constant, k, can be estimated by a dislocation pile-up model (DPM) (Meyers et al., 2006).

However, no direct experimental visualization technique is available that allows nonintrusive investigation of grain-boundary structures, limiting atomic-level understanding of grain boundaries (Swygenhoven, 2002). Liquid-like grain boundaries with the amorphous structure, resulting from cooling down from the melt, was utilized in atomistic simulation to shed light on the deformation mechanism (Swygenhoven, 2002). Hence, the glass matrix can be assimilated to grain boundaries to simplify the deformation mechanism in MGMCs. Although dislocation motion cannot be generated in the glass matrix to accommodate the plastic strain, the plastic flow in these regions at room temperature and moderate strain rates is typically inhomogeneous and proceeds via the formation and propagation of shear bands (Fornell et al., 2009; Qiao et al., 2016b).

In this study, an improved DPM is established, based on $Ti_{50}Zr_{20}V_{10}Cu_5Be_{15}$ MGMCs. The generation and multiplication of dislocations in dendrites is quantitatively assessed from the elastic to work-hardening stages to derive a relationship between the yield strength and the size of dendrites. The deformation mechanisms during the work-hardening stage are investigated by focusing on the interaction between the evolution of dislocations in dendrites and the propagation of shear bands in the glass matrix. Since the chemical composition determines the volume fraction and size of the dendrites, the dependence of the yield strength on composition is tentatively tunable, using the mean-field theory, and a universal scaling Hall-Petch-like relationship is derived successfully.

2. Experimental

Alloy ingots with a normal composition of $Ti_{50}Zr_{20}V_{10}Cu_5Be_{15}$ (atomic percent, at.%) were prepared by arc-melting the mixture of Ti, Zr, V, Cu, and Be pure metals with a purity of above 99.9% (weight percent, wt.%) and cast into a copper mold under a Ti-gettered argon atmosphere. The dimension of samples was ϕ 6 mm × 80 mm. Dog-bone-like tensile specimen gauges with dimensions of ϕ 2 mm × 15 mm were fabricated from the as-cast cylindrical samples by electrical discharge machining. Quasi-static tensile tests and pre-tensile tests were conducted at room temperature at a constant strain rate of $2 \times 10^{-4}\ s^{-1}$ for at least five times, using an Instron 6969 universal testing machine. The reloading tensile tests were defined such that the specimens were preloaded from 0 to 1400 MPa, and then reloading tests were conducted until final fracture. The phases of the as-cast samples were characterized by X-ray diffraction (XRD) using Cu Kα radiation. The microstructures of lateral and fracture surfaces of samples after tension were investigated by scanning electron microscopy (SEM). The microstructures of the samples before and after the tensile tests were analyzed by a JEM-2010 transmission electron microscope (TEM). The TEM specimens were prepared by dimpling and ion-milling, using a Gatan 691 device. A Nano Indenter II tester (MTS Systems, USA) with a trihedral Berkovich indenter was used to measure the hardness of both phases in the pre-tensile and tensile samples. The specimens were indented to a maximum depth of 500 nm at a strain rate of $0.05\ s^{-1}$, using the indenter system set in a depth-control mode. The specimens for TEM and nano-indentation tests were taken from an uniform deformation region adjacent to the softening region. In order to obtain the stress distribution near the yield point, finite-element-method (FEM) analysis, using the ABAQUS software, was performed.

3. Results

3.1. Microstructures

Fig. 1(a) shows a typical SEM image of as-cast $Ti_{50}Zr_{20}V_{10}Cu_5Be_{15}$ MGMCs, which have been processed by the image software Adobe Photoshop CC. Crystals with a dendritic morphology are uniformly distributed in the glass matrix. Analyzing Fig. 1(a), using the software Image-Pro Plus, reveals that the volume fraction of dendrites is 48 ± 1.1 (volume percent, vol.%), and the average diameter of the dendrite arms $\overline{d}$, is 2.35 ± 0.005 μm. The diameter is obtained by averaging the lengths passing through the center of the objects at 2-degree intervals for each dendrite, and at least 1000 dendrites were used for counting. The frequency counts of dendritic diameter, approximate to the Gaussian distribution, is shown in the inset of Fig. 1(a).

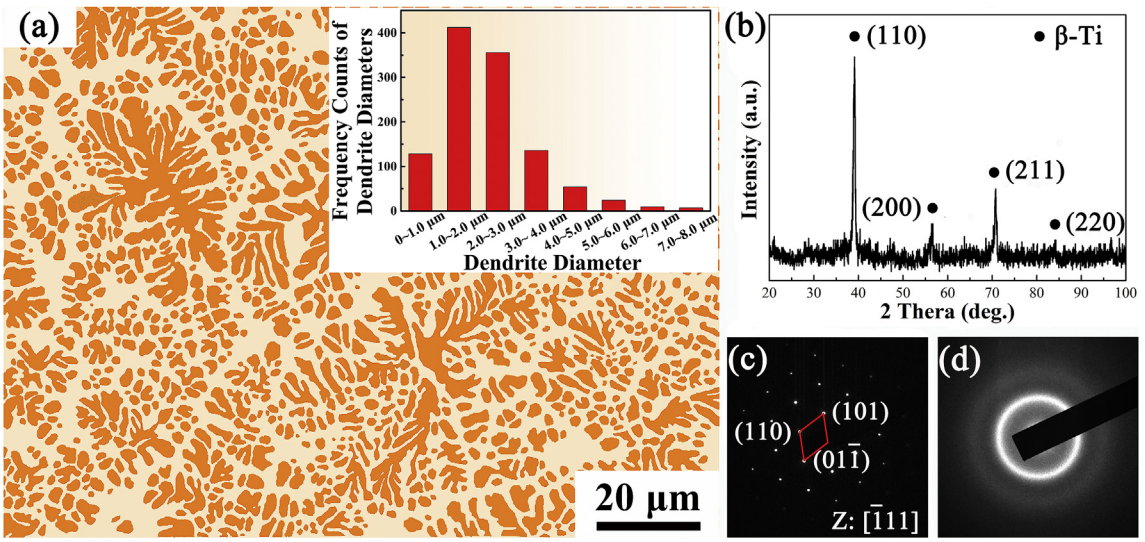

Fig. 1. (a) SEM image of the as-cast composite; (b) XRD pattern of the composite; (c) and (d) show SAED patterns of the dendrites and glass matrix, respectively.

Besides, the TEM experiments were conducted to further verify the dual-phase structure in the current composites. Characteristic selected-area electron diffraction (SAED) patterns are shown in Fig. 1(c) and (d), corresponding to the dendrites and the glass matrix, respectively. As shown in Fig. 1(c), the crystal structure of the dendrites is typically body-centered-cubic (bcc), consistent with the sharp diffraction peaks in the XRD pattern, displayed in Fig. 1(b). In contrast, only diffuse maxima appear in Fig. 1(d), revealing that the matrix has an amorphous structure.

Moreover, other *in-situ* Ti-based MGMCs with different compositions, i.e., $Ti_{40}Zr_{24}V_{12}Cu_5Be_{19}$, $Ti_{46}Zr_{20}V_{12}Cu_5Be_{17}$, and $Ti_{48}Zr_{18}V_{12}Cu_5Be_{17}$, are listed in Table 1 to identify the relationship between the yield strength and the diameter of the dendrite arms (Sun et al., 2015b; Zhang et al., 2014). Similar volume fractions of dendrites in these MGMCs were calculated from SEM images: 48 ± 2.7 vol.% for $Ti_{40}Zr_{24}V_{12}Cu_5Be_{19}$, 46 ± 0.6 vol.% for $Ti_{46}Zr_{20}V_{12}Cu_5Be_{17}$, and 54 ± 1.2 vol.% for $Ti_{48}Zr_{18}V_{12}Cu_5Be_{17}$, respectively. The average diameters of the dendrite arms are 1.08 ± 0.094, 1.36 ± 0.041, and 1.54 ± 0.053 μm, respectively.

3.2. Deformation behavior

3.2.1. Tensile properties

Uniaxial tensile tests were conducted for the as-cast MGMCs at room temperature. Fig. 2 displays a typical true tensile stress-strain curve. The curve can be divided into three stages: elastic, work-hardening, and softening stage. Obviously, the present Ti-based MGMCs exhibit a high yield strength of ~1350 MPa, and distinct work-hardening capacity (~2%), as shown in the stage (2) in Fig. 2. The ultimate tensile stress (UTS) is up to ~ 1510 MPa at a corresponding strain of ~4.2%. After achieving the ultimate stress, softening, i.e., the stage (3), prevails until the final fracture occurs at a strain of ~10.7%, accompanied by macroscopic necking of the tested samples. Analogous necking associated with tensile ductility has been found for many MGMCs (Sun et al., 2015b; Zhang et al., 2014). The inset in Fig. 2 shows the morphology of the samples before and after tension.

In order to verify that work hardening stems completely from plastically-deformed dendrites, unloading-reloading tensile tests have been conducted. Fig. 3 displays two work-hardening periods on the engineering stress-strain curve. Upon the first loading, the dendrites enter into the strengthening stage, and only a few shear bands are generated in the glass matrix (Qiao et al., 2013; Sun et al., 2015a). Compared with the yield strength upon first loading, the new yield stress upon reloading is higher than the flow stress at the point of unloading (denoted as the region A on the stress-strain curve in Fig. 3), which apparently increases by ~100 MPa. Due to the fact that dislocation motion prevails, the apparent strengthening effect during the unloading-reloading tests of the current MGMCs is consistent with other works (Wu et al., 2014; Zhang et al., 2017a).

As plastic deformation continues, a stress overshoot, i.e., a yield peak phenomenon, is widely observed in metallic glasses and

Table 1
Volume fractions of dendrites (%), average diameters, d, critical diameters, d_c, and ratios of elements, ξ, of metallic glass matrix composites.

Composition, atom (%)	Volume fraction of dendrites (%)	Average diameter, d() (μm)	Critical diameter, d_c (μm)	Ratio of elements, ξ
$Ti_{40}Zr_{24}V_{12}Cu_5Be_{19}$ (Zhang et al., 2014)	48 ± 2.7	1.08 ± 0.094	1.23 ± 0.002	3.36
$Ti_{46}Zr_{20}V_{12}Cu_5Be_{17}$ (Zhang et al., 2014)	46 ± 0.8	1.36 ± 0.041	1.28 ± 0.002	3.88
$Ti_{48}Zr_{18}V_{12}Cu_5Be_{17}$ (Sun et al., 2015b)	54 ± 1.2	1.54 ± 0.053	1.52 ± 0.003	3.88
$Ti_{50}Zr_{20}V_{10}Cu_5Be_{15}$ (Present study)	48 ± 1.1	2.35 ± 0.005	2.35 ± 0.005	4.67

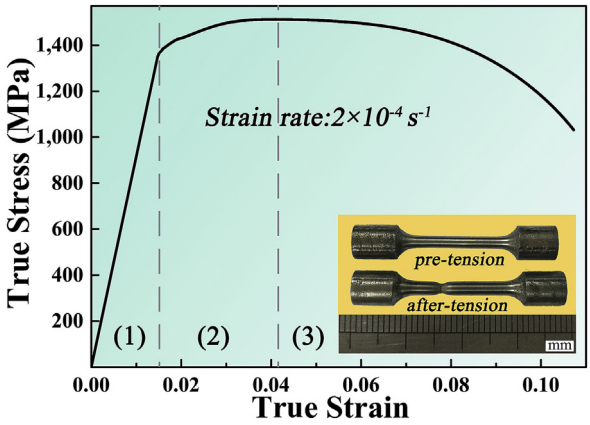

Fig. 2. Tensile true stress-true strain curve of the $Ti_{50}Zr_{20}V_{10}Cu_5Be_{15}$ MGMC.

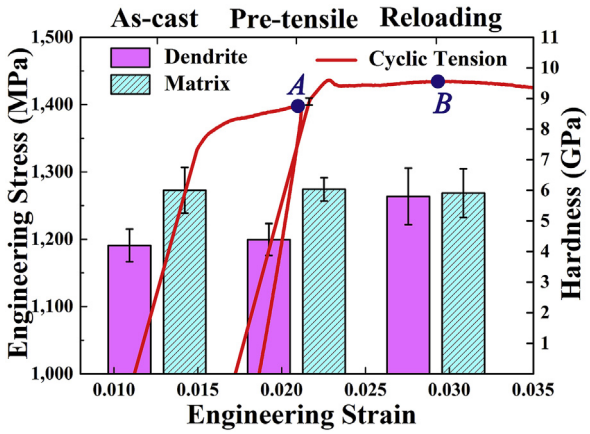

Fig. 3. Reloading the tensile engineering stress-strain curve of the composite and hardness of the dendrites and glass matrix at the three stages.

crystalline alloys (Jiang et al., 2015b; Nieh and Nix, 1986; Yang et al., 2016). The stress overshoot may be attributed to the delayed activation of shear transformations caused by the insufficient free volume in the glass matrix. The shear-induced dilatation results from the positive interplay between the shear transformation and free-volume creation, and the latter plays a dominant role (Jiang et al., 2015b). Furthermore, the co-deformation of the two phases generates an explicit elastic-plastic transition through the load transfer and strain partitioning (Eckert et al., 2011; Yang et al., 2016; Zhou et al., 2013). Upon reloading, the glass matrix is elastically deformed while the dendrites begin to deform plastically. As the tensile strain increases, the mobile dislocation density decreases within the dendrites, and a higher stress is needed to be overcome for the dendrites to yield, which lies on a forest type dislocation interaction (Nieh and Nix, 1986; Yang et al., 2016). This trend leads to an increase of the yield point. Once the glass matrix yields, the rapid relaxation of elastic stresses and strains at the interfaces between the dendrites and glass matrix causes the overall stress to drop. Therefore, the stress overshoot in the reloading tests originates from the load transfer and shear-induced dilatation in the glass matrix. After the stress drop, the samples exhibit second work-hardening up to an UTS of ~1450 MPa (denoted as the region B on the stress-strain curve in Fig. 3).

3.2.2. *Nano-indentation analysis*

In order to further explore the deformation mechanisms, nano-indentation tests on the dendrites and the glass matrix in the as-cast state, after pre-tensile deformation, and after reloading, were conducted for the present Ti-based MGMCs for at least five times, respectively. The hardness histograms in Fig. 3 display the corresponding results, as well as the comparison of the average hardness

Table 2
Hardnesses of the dendrites and the glass matrix in the as-cast state, after pre-tensile deformation, and after reloading.

Hardness (GPa)	As-cast	Pre-tensile	Reloading
Dendrite	4.2 ± 0.54	4.39 ± 0.52	5.8 ± 0.92
Glass Matrix	6 ± 0.75	6.03 ± 0.38	5.91 ± 0.80

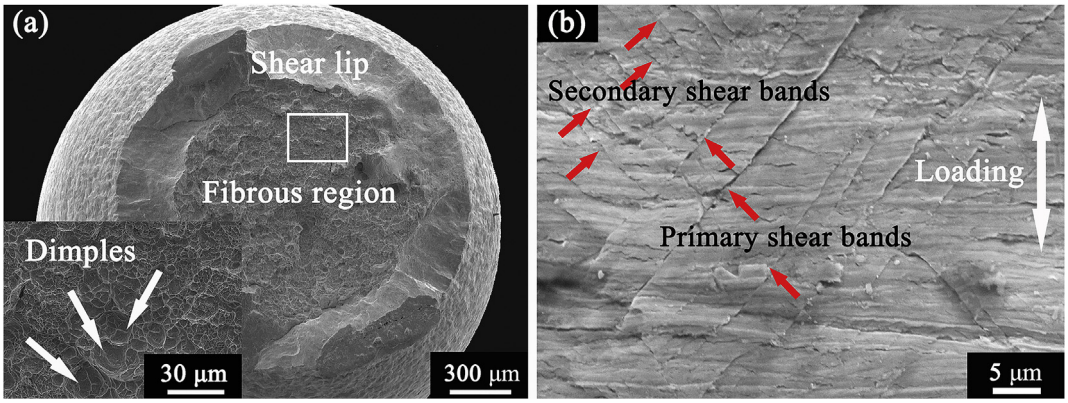

Fig. 4. Fracture (a) and lateral surfaces (b) of deformed samples after tension, respectively.

between the two phases in the very three cases. The detailed hardness values are summarized in Table 2. Obviously, the dendrites are softer than the glass matrix in the as-cast composites, as widely found for other MGMCs (Narayan et al., 2010; Wu et al., 2010; Yang et al., 2016). After the pre-tensile tests, the dendrites become slightly harder than in the as-cast state. The hardness of the dendrites successively increases due to work hardening upon plastic deformation. After the second work-hardening stage in the reloading tests, the hardness of the dendrites is almost equal to that of the glass phase. Due to a high density of shear bands with the highly-localized plasticity, the glass matrix slightly softens upon reloading (Bei et al., 2006; Hufnagel et al., 2016).

3.2.3. *Tensile deformation structure*

Fig. 4(a) shows the fracture surface consisting of shear lips and fibrous regions. Macroscopic necking can be seen, even by naked eyes, giving direct evidence for the occurrence of instable plasticity. The characteristic contour of the fracture surface, termed as a cup-and-cone fracture, is displayed in the inset of Fig. 4(a), which is a high-magnification image of the rectangle in Fig. 4(a). The dimples are indicative of ductile fracture under tension, as it frequently occurs in ductile alloys (Meyers et al., 2006). Profuse shear bands are visibly distributed on the lateral surfaces near the fracture surface, as can be seen in Fig. 4(b). The two propagation directions of the shear bands are at an angle of ~40° with respect to the loading direction. The multiplication of secondary shear bands with a spacing of 2–3 μm between the primary shear bands results from the interaction between the dendrites and the shear bands (Eckert et al., 2011).

To reveal the central role of dislocation motion on the plasticity TEM investigations were conducted. The bright-field (BF) images indicate the typical dislocation structure and multiple slip systems in the dendrites subjected to severe plastic deformation. It seems that the propagation path of the shear bands extends from the glass matrix into the dendrites. The trace of shear bands is not visible, for the reason that the formation of shear bands is not dominated by the crystallization (Chen and Lin, 2010). Diffraction pattern in Fig. 5 show that the microstructure of the glass matrix remained amorphous after tension. Plenty of dislocation glide lines are parallel and transect the dendrites. According to the $[11\bar{1}]$ orientation of the selected area electron diffraction (SAED) pattern shown in the inset of Fig. 5(a), two direction glide lines are perpendicular to the $(01\bar{1})$ and $(12\bar{1})$ planes, respectively, as unveiled by the trace analysis. The dislocation glide inside the dendrites is localized on a distinct set of {110}/{121}-type bcc lattice planes. Another two direction glide lines are perpendicular to $(0\bar{1}1)$ and $(\bar{4}1\bar{4})$planes, as shown in Fig. 5(b). Some slip systems are activated not only on the preferred planes {110}, but also on {121} and {414}-type bcc lattice planes. In contrast to the SAED patterns from as-cast MGMCs, only the dislocation-based model of plastic deformation has taken place in the dendrites during tension. Even though the dendrites

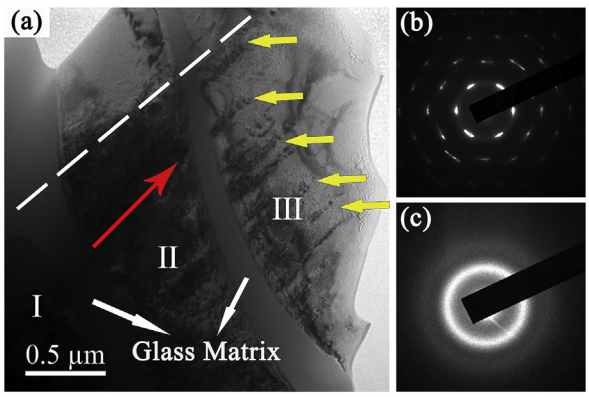

Fig. 5. TEM bright-field image of the typical dislocation structure and the multiple slip systems in the dendrites after tension.

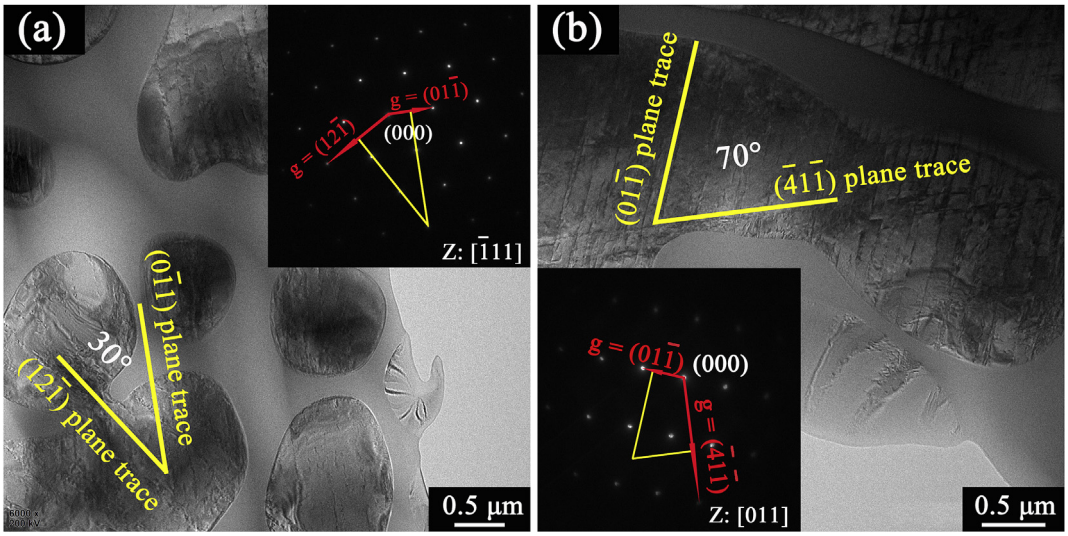

Fig. 6. (a) TEM bright-field image of the deformed composites after tension. The SAED patterns of the dendrites and the glass matrix are shown in (b) and (c), respectively.

suffer a high stress concentration, neither twinning nor phase transformation behavior is discovered in the current composites. Apparently, the addition of a considerable amount of vanadium as the β-phase-stabilizing element accounts for this dislocation-based deformation mode (Hofmann et al., 2008b; Kolodziejska et al., 2016; Zhang et al., 2017a, 2017b; Zhecheva et al., 2005).

Fig. 6(a) displays a TEM BF image to visually elaborate the stress propagation in the MGMCs. The areas I, II, and III of the BF images correspond to dendrites that keep the same crystal orientation, and the area between these three areas is the glass matrix. This trend can be confirmed by the SAED patterns, shown in Fig. 6(b) and (c). Below the dashed line in Fig. 6(a), the propagation path of shear bands (denoted by yellow arrows) can be observed. Shear bands penetrate the whole dendrites. The direction of their propagation path is indicated by red arrows. Furthermore, above the dotted line in the BF image, the dislocation lines are invisible in areas II and III, owing to the shortage of area I. Obviously, shear bands initiate from area I, go through area II, and are terminated in area III, which proves that the rapid propagation of shear bands has been effectively stopped.

To sum up, a clear survey of dislocation lines gliding on other planes except the close-packed planes confirms that dendrites have been hardened to a great extent. This feature explains the strong hardness increase with increasing strain. The highly-strengthened dendrites also promote many secondary shear bands, as shown in Fig. 4(b) (Qiao et al., 2011; Song et al., 2016; Wu et al., 2011). These branched secondary shear bands consume part of the stored elastic energy, avoiding primary shear bands to propagate across the whole shear plane (Wang et al., 2009). The formation and propagation of profuse secondary shear bands produces more plasticity in the glass matrix, in agreement with the pronounced tensile ductility (Wang et al., 2004, 2009). Double slip is widely identified in Fig. 5 due to the fact that the critical shear stress is simultaneously approached on these slip planes. The pronounced multi-slip activity reveals that the applied shear stress is large enough to operate several slip systems. The high applied shear stress lies in the range of the high critical deformation stress for the glass matrix. Meanwhile, the operation of several slip systems within the dendrites supplies higher resistance to the extension of shear banding. The distinct work hardening and ductility of the present Ti-based MGMCs can be ascribed to this strong resistance to the propagation of shear bands (Hofmann et al., 2008a; Qiao et al., 2011; Song et al., 2016; Wu et al., 2011).

3.2.4. Stress distribution

To further understand the process of dislocation motion, the strain field determined by the FEM analysis demonstrates different dispersion characteristics for samples that are plastically deformed to the same strain of 1%. At this moment, the dendrites have to enter the plastic stage, while the glass matrix stays in the elastic stage. The stress distribution contour map is schematically displayed in Fig. 7. The ellipses represent dendrites, and other area in between is the glass matrix. The Young's modulus of dendrites and the glass matrix used in the FEM analysis are obtained from nano-indentation tests yielding values of 96 ± 2.6, and 128 ± 2.8 GPa, respectively. The Poisson's ratios of dendrites (ν_d = 0.33) and the matrix (ν_m = 0.30) are obtained from previous studies (Qiao et al., 2013). As can be seen in Fig. 7, the stress concentration happens at the interface, consistent with our current and previous experimental findings (Hofmann et al., 2008a; Qiao et al., 2013), which manifests the location of the dislocation sources. Due to the mismatch of the plastic deformation in the dendrites and the elastic deformation in the glass matrix, these dislocations easily propagate along the direction of the shear stress and pile up. Moreover, this map also indicates that the interface is the preferable site for shear-band initiation (Sun et al., 2016). Due to the formation and accumulation of dense dislocations within the dendrites, strain hardening occurs. Once the shear stress due to dislocation pile-up within dendrites reaches the yield strength of the glass matrix, shear bands initiate at the interface.

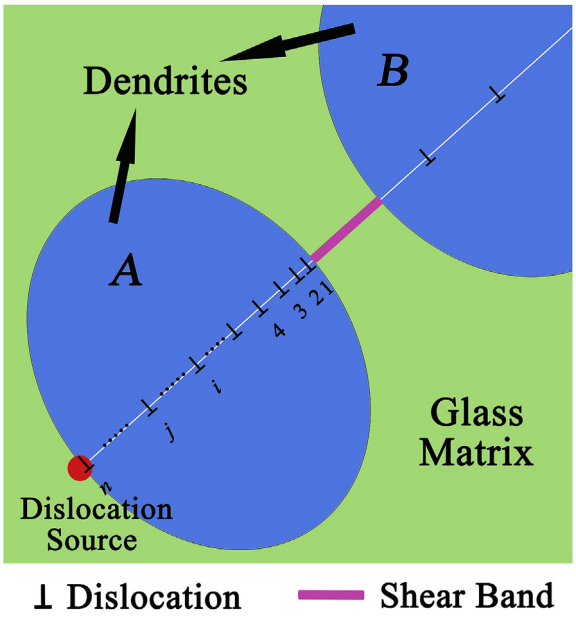

Fig. 7. Contour maps of the stress distribution at the moment of yielding of dendrites.

4. Discussion

4.1. Tensile yielding

As the dendrites can impede the rapid propagation of shear bands and promote the multiplication of shear bands, the soft dendrites play a vital role in enhancing the tensile ductility of the present Ti-based MGMCs (Eckert et al., 2011; Hofmann et al., 2008a; Qiao et al., 2009a, 2011, 2012, 2013, 2016a; Sun et al., 2015a; Zhang et al., 2014). Compared with typical monolithic BMGs, which exhibit strain softening, the addition of *in-situ* dendrites into the glass matrix is capable of avoiding shear localization leading to the catastrophic failure (Eckert et al., 2011; Hofmann et al., 2008a; Qiao et al., 2011, 2016a). Meanwhile, compared with their crystalline counterparts, the Ti-based MGMCs show a higher strength on account of the great strength of the glass matrix (Hofmann et al., 2008b; Wang et al., 2004; Yoo et al., 2012). Hence, the plastic-deformation mechanisms in the current composites are tightly coupled with the pile-up dislocations in dendrites and shear banding in the glass matrix.

In order to reveal the deformation mechanisms, a dislocation pile-up model (DPM) is established according to the dislocation motion within dendrites and shear banding in the glass matrix. As schematically shown in Fig. 7, the dislocation pile-ups in the blue area (dendrite A), together with the generation and propagation of shear bands in the green area (glass matrix), microscopically promulgate the process during plastic deformation. On the elastic stage, the mismatch of the yield strength and Young's modulus of both phases leads to the incongruous deformation (Qiao et al., 2011, 2013; Sun et al., 2015a). Microscopically, when the tensile stress increases to the yield strength of the dendrites, dislocations initiate from the interface, and then, these dislocations slip along the favorable direction within the dendrites, while the glass matrix remains in the elastic stage (Oh et al., 2011; Şopu et al., 2015; Zhou et al., 2013). Thereafter, as the applied stress continuously increases, many dislocations are generated from the dislocation sources at the interface, and move along the direction of shear banding and pile up at the interface (Ma et al., 2014). Through this arrangement, corresponding to Fig. 7, a higher stress concentration arises at the interface (Zhang et al., 2014).

Similar to polycrystalline alloys, the macroscopic plasticity in MGMCs is caused by the fact that the dislocation slip occurs in many crystals. The yielding of the MGMCs occurs because the increase of the applied stress results in dislocation motion in the adjacent crystals. When the shear stress is larger than the yield strength of the glass matrix, shear bands nucleate near the interface, and propagate rapidly until reaching the adjacent dendrites (Greer et al., 2013). At this moment, plastic deformation has penetrated through several interfaces and is transmitted among dendrites. Here, the applied normal stress is defined as the yield strength of the MGMCs.

From these considerations, the schematics of the deformation at the yield point can be constructed, referring to the dislocation lines on the TEM images. When the applied shear stress, τ^*, is approaching the critical value, the first dislocation is driven from the dislocation source and propagates along the direction of shear banding. Until this dislocation is blocked by an interface, the dislocation source will generate the next dislocation. According to the DPM, each dislocation suffers the force that comes from foregoing dislocations, resulting in the distance between the adjacent dislocations becoming longer and longer. The jth dislocation is in equilibrium when experiencing the applied stress, τ^*, and the resultant force, F, from other dislocations. The force, F_j, which the jth dislocation experiences, is given by (Nabarro, 1947):

$$F_j = \frac{Gb^2}{2\pi} \sum_{\substack{i=1 \\ j\neq i}}^{n} \frac{1}{x_j - x_i} = \tau^* b, \tag{1}$$

where G and b are the shear modulus and Burgers vector of the dendrites, respectively, and x_i is the distance from the ith dislocation to the first dislocation.

The equilibrium equation of the dislocation pile-up group can be calculated, based on the location of each dislocation, which is expressed according to Eq. (1),

$$\frac{\tau^*}{D} = \sum_{\substack{i=1 \\ i\neq j}}^{n} \frac{1}{x_j - x_i}, \tag{2}$$

where$D = \frac{Gb}{2\pi(1-\nu_d)}$. As shown in Eq. (3), the position of each dislocation can be obtained by solving the n equations with n unknowns $(x_j - x_i)$ for the dislocations behind the lead dislocation in Eq. (2). This derivation was introduced by Eshelby et al. (1951), and the result is presented without derivation.

$$x_n = \frac{\pi^2 D}{8n\tau^*}(n-1)^2 \tag{3}$$

Due to the source of the dislocation is located at the interface of the grain, the distance from the nth dislocation to the first dislocation, x_n, is equal to the diameter of the dendrite arms, d. Considering that the number of dislocation pile-ups, n, is far above 1, Eq. (3) can be simplified as Eq. (4).

$$x_n \approx \frac{\pi^2 Dn}{8\tau^*} \approx d \tag{4}$$

Equation (4) explains that upon the same stress, more dislocations will be accumulated within the interior of dendrites with larger sizes. The more dislocations are generated, the larger stress the interface will suffer. In polycrystalline alloys, the interfaces, which can impede the motion of dislocations effectively, play a key role on strengthening alloys (Li et al., 2010). Here, the glass matrix has a similar function but a stronger effect than the grain boundaries, since the critical deformation shear stress of the glass matrix, f', is very high, owing to the unique amorphous structure. The interfaces suffer the shear stresses caused by the dislocation pile-ups (Oh et al., 2011). Jang et al. (2010) have reported that a highly-localized-to-homogeneous deformation mode change occurs at a diameter of 100 nm, without any change in the yield strength. Although the thicknesses of the glass matrix between dendrites are quite different, the critical resolved shear stress can be considered as a constant.

When the shear stress is smaller than the critical deformation shear stress of the glass matrix, f', the adjacent dendrite B (Fig. 7) benefits from the resistance of the glass matrix to prevent further plastic deformation. Once the shear stress reaches f', shear bands are generated immediately and extend rapidly until they are impeded by the dendrite B. Then the plastic deformation transfers to another dendrite, accompanied by the formation of shear bands. Therefore, the interface for dendrites with a larger size exhibits a lower applied shear stress, τ^*, which causes the earlier nucleation of shear bands in the glass matrix (Şopu et al., 2015). Consequently, in-situ MGMCs with smaller dendrite sizes exhibit higher yield strengths. This deduction is generally confirmed by earlier studies, including Ti- (Hofmann et al., 2008a, 2008b; Zhang et al., 2014; Wang et al., 2015), Zr- (Cheng et al., 2010; Jeon et al., 2012, 2013, 2016; Kolodziejska et al., 2016), Mg- (Gao et al., 2015; Wang and Xu, 2013), and La-based (Wang et al., 2009) MGMCs.

The establishment of the DPM relays on the interaction between dislocation lines. The critical shear stress, τ_c, which can cause the dislocation motion in the dendrite B (Fig. 8), is described by Eq. (5). Once initiated, shear bands are prone to becoming unstable due to strain softening and propagate rapidly in the glass matrix, accompanying a sudden stress drop at the period of the early deformation (Chen and Dai, 2016; Qiao et al., 2016b; Sun et al., 2016; Wang et al., 2009; Zhao et al., 2013). Compared to the yield strength of MGMCs, the stress drop can be neglected (Antonaglia et al., 2014; Wang et al., 2009). Hence, τ_c is equal to f'.

When the first dislocation moves forward by a small distance, δx, so do the others. Owing to the dislocation pile-up, n dislocations along the direction of the dislocation line block. The applied shear stress, τ^*, does the work per unit length of dislocation, as given by $nb\tau^*\delta x$. When experiencing the applied stress of the first dislocation, τ_1^*, the increase in the energy of the first dislocation is $b\tau_1^*\delta x$. In equilibrium, $\tau_1^* = n\tau^*$.

$$\tau_c = f' = \tau_1^* = n\tau^* \tag{5}$$

Upon cooling from the high-temperature melt, in-situ MGMCs undergo the nucleation and subsequent growth of dendrites in the remaining liquid (Qiao et al., 2016a). Lattice defects are rarely found in the as-cast state (Qiao et al., 2011). Therefore, the contribution from redundant dislocations can be neglected (Hansen, 2004). Combining Eqs. (3) and (4) together with the Hall-Petch-like relationship, the relationship between the applied shear stress, τ, and the diameter of dendrite arms, d, is determined by the following equation,

$$\tau = \tau_0 + \frac{\pi}{4}\sqrt{2D\tau_c}\, d^{-1/2}, \tag{6}$$

where τ_0 reflects the resistance to hinder the plastic deformation within the interior of the dendrites. Apparently, there is a linear relationship between the applied shear stress, τ, and the inverse square root of dendrite arms, $d^{-1/2}$.

The Schmid factor of dendrites, m, is considered in the relationship between the normal stress and the shear stress upon uniaxial

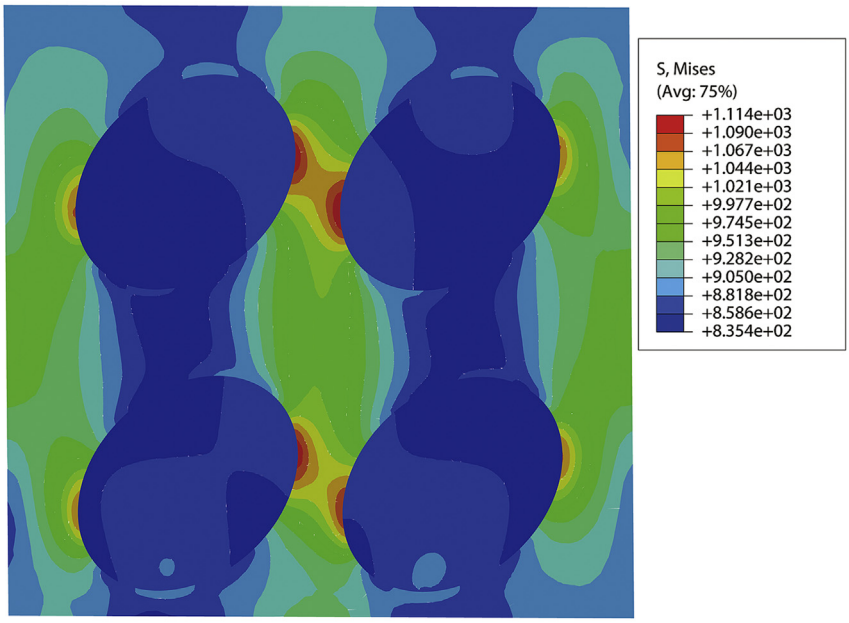

Fig. 8. Schematic illustration of the dislocation pile-up model in MGMCs and dislocation motion at the yield point.

tension. The normal stress can be written as:

$$\sigma = \sigma_0 + kd^{-1/2}, \tag{7}$$

where k is a materials constant, with $k = \frac{\pi}{4m}\sqrt{2D\tau_c}$. The normal stress, σ_0, is a constant, which can be interpreted as the lattice friction in dendrites.

Finally, combining the Hall-Petch-like relationship derived by the DPM with the properties of two phases, the relationship between the yield strength and the dendrite size in the current MGMCs have been built. MGMCs have a dual-phase microstructure by introducing secondary phases into the metallic glass. The volume fraction of the glass matrix is over the half of composites. The width of the glass matrix ranges up to several micrometers and even exceeds the diameter of a portion of dendrites. In addition, differing from leading dislocation driven by the shear stress to traverse the grain boundary in polycrystalline alloys, the glass matrix in MGMCs cannot transfer dislocations due to the amorphous structure. Therefore, this Hall-Petch-like behavior is a composite yielding phenomenon. The behavior originates from the fact that the dislocation pile up is the controlling/triggering event and dependent on the dendrite size and the critical deformation stress of the glass matrix, f'.

Next, the activation of multiple slip systems is taken into consideration, which is common during the plastic deformation of crystalline alloys, as shown in Fig. 7 (Bishop and Hill, 1951; Hashimoto and Margolin, 1983). When the shear stress simultaneously approaches the critical shear stress on two of the possible planes and directions, double glide can be activated. As the close-packed planes of atoms in bcc dendrites, two slip planes (110) and (112) of these possible planes are studied, and the dislocation slip direction in slip planes is [111]. Although the crystalline aggregate of dendrites is isotropic, the individual dendrite exhibits the elastic anisotropy characteristic of the crystal symmetry. In order to determine the elastic modulus undergone by the monocrystalline cubes, it is convenient to convert the elastic constants into an effective elastic modulus (Meyersm and Ashworth, 1982). The determination of Young's modulus of single crystals is described by Eq. (8).

$$\frac{1}{E_{ijk}} = S_{11} - 2\left(S_{11} - S_{12} - \frac{1}{2}S_{44}\right)(l_i^2 l_j^2 + l_j^2 l_k^2 + l_i^2 l_k^2) \tag{8}$$

where E_{ijk} is Young's modulus along the [ijk] direction, S_{11}, S_{12}, and S_{44} are the compliances of the dendrites and l_i, l_j and l_k are the direction cosines of the [ijk] direction with respect to the crystal axes. Compliance constants of this Ti-based dendrites are the same as the unalloyed titanium as an approximation, $S_{11} = 0.998 \times 10^{-11} Pa^{-1}$, $S_{12} = -0.471 \times 10^{-11} Pa^{-1}$, (Meyersm and Ashworth, 1982). Hence, the elastic modulus along the [111] slip direction, E_{111}, is 197.9 GPa. Combining with the relationship between the Young's modulus and the shear modulus, G, in dendrites $G = \frac{E_{111}}{2(1+\nu_d)}$, and the materials constant, k, can be expressed as:

$$k = \frac{1}{2m}\sqrt{\frac{\pi E_d \tau_c b}{2(1+\nu_d)(1-\nu_d)}}. \tag{9a}$$

where b is the Burgers vectors and $b = \frac{a}{2}\langle 111\rangle$.

The yield strength, obtained from the macroscopic uniaxial yield shear stress, is 2.2τ. Here, τ is the shear yield stress of a single crystal (Bishop and Hill, 1951), whereas, the crystallographic orientation of the dendrites varies from grain to grain, analogous to

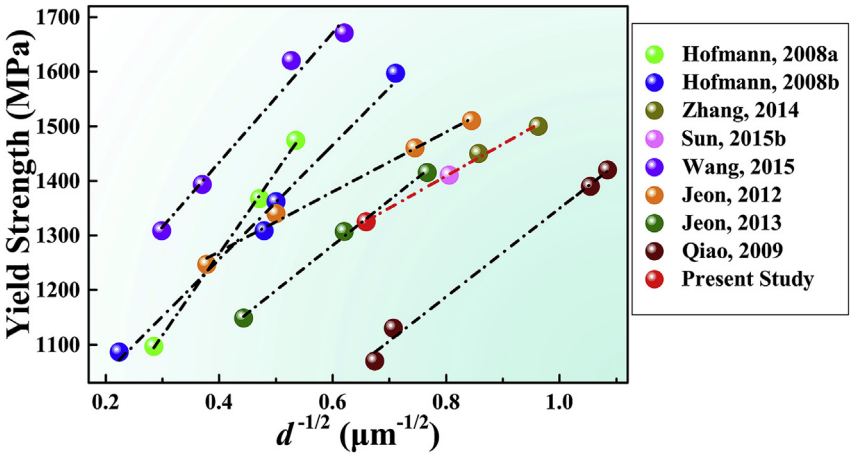

Fig. 9. Linear relationship between the yield strength and the inverse square root of the average dendrite size.

polycrystalline alloys (Kolodziejska et al., 2016). Bishop and Hill have pointed out that the best fit of the Schmid factor in polycrystalline alloys, m, based on the Taylor's model, gives a value of about 0.3 (Bishop and Hill, 1951). Then τ_c can be calculated, $\tau_c = E_m \varepsilon_{2\%} \cos\theta$. In the metallic glass, θ is the angle under that the shear stress is oriented (Lewandowski and Lowhaphandu, 2002; Qiao et al., 2016a).

For the current Ti-based MGMCs, the lattice constant of the dendrites, obtained from previous studies, is 0.3203 nm (Qiao et al., 2011). According to Eq. (9b), the material constant, k_c, is 0.43 MPa m$^{-1/2}$, close to the experimental material constant, k_E = 0.58 MPa m$^{-1/2}$, as shown in Fig. 9.

This relationship between σ and $\overline{d}^{-1/2}$ can be verified for many other in-situ MGMCs, as demonstrated in Fig. 9 (Hofmann et al., 2008a, 2008b; Jeon et al., 2012, 2013; Qiao et al., 2009b; Wang et al., 2015; Zhang et al., 2014). In all these MGMCs, the dendrite size is controlled by the variation of composition and cooling rate (Jeon et al., 2012; Qiao et al., 2009b; Zhang et al., 2014; Wang et al., 2015). The value of k varies for different compositions and preparation methods, such as the copper mold suction casting and Bridgman solidification, as shown in Fig. 9.

Nevertheless, the linear relationship has limitations, and is only suitable for in-situ MGMCs with stable dendrites. The plastic deformation in such composites is only dominated by the multiplication of dislocations. The MGMCs reinforced by B2 (CuZr) phases or metastable β phases are not considered in this study on account of the deformation-induced phase transformation and twinning (Wu et al., 2010, 2011; Zhang et al., 2017b). Transformation-induced plasticity (TRIP) and twin-induced plasticity (TWIP) are effective methods for plasticity improvement, due to the fact that the local strain in β dendrites is largely released (Hofmann, 2010; Song et al., 2016; Wu et al., 2011; Zhang et al., 2017b). Hence, the case in MGMCs reinforced by stable dendrites is different from that reinforced by B2 phases and metastable dendrites. For this reason, this model is not suitable for in-situ MGMCs reinforced by B2 phases and metastable dendrites.

Moreover, the tensile-deformation model of MGMCs with different sizes of dendrites indicates that the dendrite size can become so small that it may lead to the brittle fracture (Zhang et al., 2014). It is crucial for MGMCs to have suitably-sized dendrites so that dislocation slip can occur in the dendrites (Oh et al., 2011; Zhang et al., 2014). Hence, the applicability of this linear relationship depends on the critical size and volume fraction of dendrites in the same MGMCs.

4.2. Mean-field theory for the diameter of dendrites

The sizes of the dendrite arms are different for varying compositions in Ti-Zr-V-Cu-Be MGMCs. The constituent elements, Ti, Zr, and V, readily form a solid solution, while Be and Cu have the limited solubility in the dendrites (Hofmann et al., 2008b). The volume fraction of dendrites is essentially determined by the ratio of these two groups of elements, $\frac{\text{Ti + Zr + V}}{\text{Cu + Be}}$(atom %), i.e., the atomic percentage of low solubility elements in MGMCs (Hofmann et al., 2008b; Kolodziejska et al., 2016). The amount of V varying from near the zero-percent to twelve percent in Ti-based MGMCs has less impact on the size of the dendrite arms (Kolodziejska et al., 2016). Therefore, in this study, a small change in the amount of V has a minimal effect on the diameter of the dendrite arms, and the amount of Cu is kept constant in the four investigated compositions. Thus, the ratio of the atomic% of Ti plus Zr to Be, $\xi = \frac{\text{Ti + Zr}}{\text{Be}}$(atom %), can be supposed to a variable influencing the diameter of the dendrite arms.

The yield strength of MGMCs is not only determined by the dendrite size but also the volume fraction. Hence, when discussing the dependence of dendrite sizes to the ratios of the percentage of Ti and Zr over Be, ξ, the atomic percentage of low solubility elements in MGMCs should be kept constant to ensure the same volume fraction of dendrites. In this study, the series of compositions of $Ti_{40}Zr_{24}V_{12}Cu_5Be_{19}$, $Ti_{46}Zr_{20}V_{12}Cu_5Be_{17}$, $Ti_{48}Zr_{18}V_{12}Cu_5Be_{17}$, and $Ti_{50}Zr_{20}V_{10}Cu_5Be_{15}$ MGMCs have the similar ratio of these two groups of elements. The volume fractions of dendrites of MGMCs, listed in Table 2, are also equal approximately.

Based on these considerations, a quantitative analysis for the influence of composition on the size of dendritic diameters in MGMCs is conducted. In Fig. 10, the ergodic evolution of the diameter of dendrite arms, d, demonstrates that a complementary

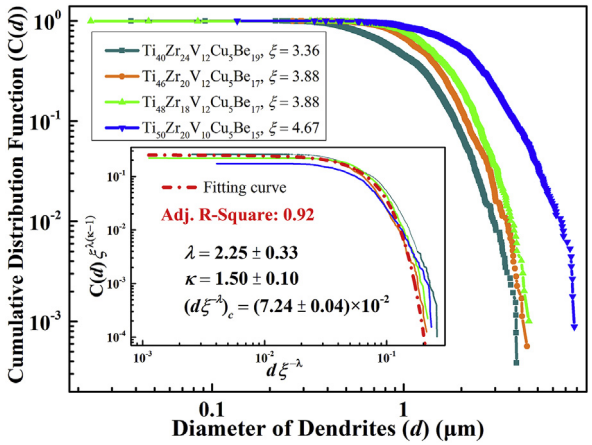

Fig. 10. Complementary cumulative distribution functions (CCDFs) of the diameters of the dendrite arms in Ti-Zr-V-Cu-Be MGMCs. The inset shows the universal collapse scaling according to Eq. (9a). The dash-dotted line corresponds to the fitted collapse scaling function.

cumulative distribution (CCD), i.e., the percentage of the number of dendrites with a diameter larger than a diameter, C ($\geq d$), is nonlinearly dependent on the value of d. According to the double logarithmic curves, it is obvious that smaller diameters follow a power-law distribution, while the larger diameters do not follow a power-law distribution, but decrease exponentially in probability. The complementary cumulative distribution functions (CCDFs) for the dendrite sizes in the MGMGs follow a universal scaling function, which can be approximated well by a power-law distribution function accompanied with a squared exponential decay function (Qiao et al., 2016b; Tong et al., 2016; Wang et al., 2009):

$$C(d) = Ad^{-\beta} \exp[-(d/d_c)^2] \tag{9b}$$

where A is a normalization constant, β is a scaling exponent, and d_c is the critical diameter of the dendrite arms. The critical dendrite arm diameter, d_c, is obtained by fitting the experimental data according to SEM images, which extends over a large range of dendrite diameters following a power-law distribution before turning to the exponential decay. This trend reflects that the scale-free system self-organizes into a critical state (SOC) (Bak et al., 1987; Wang et al., 2009). As listed in Table 1, the d_c values in these MGMCs are very close to the average diameters.

A mean-field theory (MFT) model predicts the complementary cumulative distribution function (CCDF), $C(d)$, of the diameter of dendrite arms, d, to indicate the dependence of the diameter to the ratio, ξ, as shown in the inset of Fig. 10 (Denisov et al., 2016). CCDF is useful for systems with a small number of dendrites (Antonaglia et al., 2014).

$$C(d, \xi) = \xi^{\lambda(\kappa-1)} C'(d\xi^{-\lambda}) \tag{10}$$

Here, $C'(d\xi^{-\lambda})$ is a universal scaling function. In MFT, the maximum observed dendrite diameter, $d_{\max}$, depends on the ratio as $d_{max} \sim \xi^{-\lambda}$(Antonaglia et al., 2014). Furthermore, $\kappa = 1.50$, $\lambda = 2.0$ are predicted very well (Antonaglia et al., 2014; Wang et al., 2009). The two exponents are carefully tuned until the curves lie on top of each other. Combined with fitting the universal scaling collapse, $C'(x) = A'd^{-\beta'} \exp[-(x/x_c)^2]$, it is found that $\kappa = 1.50 \pm 0.10$, $\lambda = 2.25 \pm 0.33$, and $x_c = (7.24 \pm 0.04) \times 10^{-2}$μm in the MFT model for the collapses in these MGMCs. Error bars for the exponents indicate that the range of exponents agrees with the model prediction using the MFT. x_c can be considered as a universal characteristic value that links the critical diameters, d_c, to ξ. Besides, $x_c = d_c\xi^{-\lambda}$ is well established with the universal scaling collapse, $C'(d\xi^{-\lambda})$. Therefore, the values of d_c for other ξ can be predicted. Considering the same composition but varying cooling rates, the dendrite sizes vary in MGMCs (Jeon et al., 2012, 2016; Wang et al., 2015). Hence, the constants, d_c and λ, remain invariable for the same cooling rate and element compositions in the prediction.

Combing with Eq. (9a,b), and based on the values of k and ξ, the yield strength of Ti-based MGMCs can be predicted as well, expressed as follows:

$$\sigma = \sigma_0 + \frac{1}{2m}\sqrt{\frac{\pi E_{111}\tau_c b}{2(1+\nu_d)(1-\nu_d)}}\,(x_c\xi^{\lambda})^{-1/2} \tag{11}$$

This relationship between σ and ξ in the Ti-Zr-V-Cu-Be MGMCs is well demonstrated in Fig. 11. The green dash-dotted line is fitted well with the experimental value, and the slope $k_E = 0.58$ MPa m$^{-1/2}$. According to the experimental slope, the yield strength of the Ti-Zr-V-Cu-Be MGMCs can be accurately predicted. The relationship derived theoretically still has a little error (~2%), as expressed by the red dash-dotted line. Nevertheless, it can be used to estimate the yield strength of MGMCs conveniently and quickly. As an additional limitation, in order to predict accurately, an experiment for one of these MGMCs is also needed to correct the value of the normal stress, σ_0.

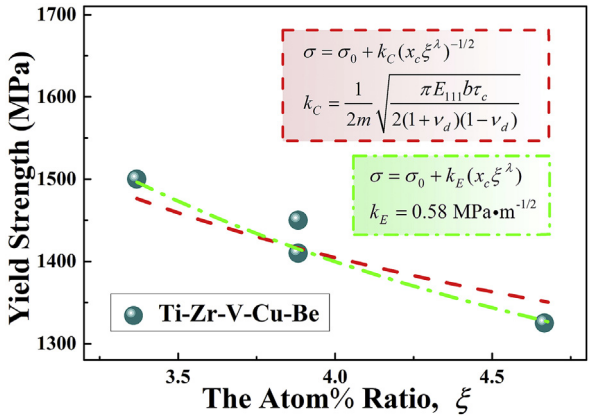

Fig. 11. The curves of the relationship between the yield strength, σ_y, and the atomic % ratio of Ti plus Zr to Be, ξ, in Ti-Zr-V-Cu-Be MGMCs.

4.3. The dependence of volume fraction of metallic glass on yield strength of MGMC

The glass matrix in MGMCs cannot transfer dislocations and plastic deformation in metallic glasses is generally associated with inhomogeneous flow in highly-localized shear bands (Eckert et al., 2011; Wang et al., 2009). Once the shear stress, concentrating on the interface, reaches the critical deformation stress of the glass matrix, *f'*, shear bands are prone to becoming unstable and propagate rapidly, accompanying a sudden stress drop (Antonaglia et al., 2014; Wang et al., 2009). The stress drop can be neglected because the stress drop is too smaller than the critical deformation stress of the glass matrix, *f'*. Shear bands extend rapidly until they are impeded by another dendrite and the plastic deformation transfers to another dendrite (Eckert et al., 2011; Hofmann et al., 2008b; Qiao et al., 2011). Based on this consideration, the dislocation pile-up model of MGMC has been established. So far, the yield strength of MGMC seemingly depends on dendrite and the critical deformation stress of the glass matrix, *f'*, insteading of the volume fraction of glass matrix. However, the multiplication of shear bands in the glass matrix must be considered into the discussion of the dependence of volume fraction on yield strength (Eckert et al., 2011).

SEM observations of surfaces of deformed samples reveal a high density of shear bands, organized in two networks: primary shear bands and secondary shear bands, i.e., the multiple shear bands, as shown in Fig. 4(b). Intersection and interaction between the two patterns of shear bands as well as multiple branching and bifurcation are found. The formation of multiple shear bands impede the extension of subsequent shear bands effectively, which contributes to the improved plasticity in metallic glass (Eckert et al., 2011; Hofmann et al., 2008b).

At the yield point of deformed MGMC, the glass matrix has entered into the plastic-deformation period and multiple shear bands have generated extensively. The larger the volume fraction of glass matrix is, the more interactions of shear bands generate. Due to the contribution of the intersection and interaction on impeding the extension of subsequent shear bands, the MGMC with larger the volume fraction of glass matrix performs higher strength. It needs to be emphasized that the multiplication of shear bands is not abundant in glass matrix on account of the early period of deformation.

Therefore, when keep the size of dendrites constant, the MGMC with larger the volume fraction of glass matrix performs higher yield strength. The influence of volume fraction on yield strength of MGMC is slighter than that of the size of dendrites.

4.4. The work-hardening stage

The strengthening effect upon reloading leads to an improvement of the yield stress, which verifies the distinct work-hardening capacity (Yang et al., 2016; Zhu et al., 2016). Since the glass matrix has been entering the softening stage, the apparent improvement of the yield stress is rooted in the strain strengthening of dendrites (Qiao et al., 2011, 2013; Sun et al., 2015a).

During plastic deformation, the explanation for work hardening before Point B (Fig. 3) on the stress-strain curves are as follows: (i) A stress concentration occurs near the interface through dislocation pile-ups, which causes the formation of multiple shear bands in the glass matrix (Eckert et al., 2011; Qiao et al., 2009c; Zhang et al., 2017b; Zhou et al., 2013), as demonstrated in Fig. 4(b); (ii) The shear bands spread from the glass matrix into the dendrites in the form of dislocation lines and are impeded by the resistance from the movement and entanglement of dislocations (Sun et al., 2015a; Zhou et al., 2013), as demonstrated in Fig. 6(a).

The hardness of the dendrites and glass matrix, characterized by the nano-indentation analysis, varies with the strain in the work-hardening stage. Compared with that of as-cast samples, the hardness of the dendrites after pre-tensile deformation presents a slight increase of 190 MPa, which elucidates that the dendrites have not been strengthened strongly. According to the strengthening effect, a large number of dislocations are mainly distributed near the interfaces, consistent with the DPM. This is the reason why the hardness of the dendrites is similar to that of the as-cast state, and also verifies that the inhibition of dislocation motion through the interface is the key to the work-hardening stage in MGMCs (Qiao et al., 2009c, 2011). Upon further plastic deformation, a remarkable hardness increase in the dendrites after reloading is indicative of a strain-strengthening effect. A dense array of dislocations has been generated and entangled inside the dendrites, which contributes to the further increase of the tensile strength in the present MGMCs.

5. Conclusions

In summary, crystalline dendrites play a significant role for the tensile yield strength and work-hardening behavior of in-situ MGMCs. A dislocation pile-up model (DPM) has been established to analyze the effect of the size of dendrite arms and the dislocation motion at the yield point. In the early stage of plastic deformation, due to the DPM, the dislocations are blocked by the interface so that the hardening effect in the dendrites is not obvious. As the deformation continues, the multiplication and entanglement of dislocations promote the retardation of the propagation of shear bands effectively, and the tensile strength of the composites is enhanced in the work-hardening stage.

Composites with smaller dendrite arms exhibit higher yield strengths in the same alloy system, whose plasticity is only dominated by dislocations. For similar volume fractions of dendrites, there is a linear Hall-Petch-like relationship between the yield strength, σ_y, and the inverse square root of the diameter of dendrite arms, $d^{-1/2}$, in these composites. The materials constant, k, in this linear relationship can be calculated on the basis of materials parameters of the MGMCs. The mean-field theory can be utilized to predict the critical diameter of dendrite arms of MGMCs with the similar atomic percentage of low solubility elements, d_c, which is influenced by the ratio, ξ. Altogether, the present work provides a quantitative relationship for predicting the yield strength of *in-situ* dendrite-reinforced MGMCs, conveniently and precisely.

Acknowledgements

J.W.Q. would like to acknowledge the financial support of the National Natural Science Foundation of China (No. 51371122), and the Youth Natural Science Foundation of Shanxi Province, China (No. 2015021005). P.K.L. would like to acknowledge the National Science Foundation (DMR-1611180), the Department of Energy (DOE), Office of Fossil Energy, National Energy Technology Laboratory (DE-FE-0008855, DE-FE-0024054, and DE-FE-0011194), with Dr. Farkas, Mr. V. Cedro, Mr. R. Dunst, and W.J. Hullen as program managers. J.E. would like to acknowledge support through the ERC Advanced Grant INTELHYB (grant ERC-2013-ADG-340025).

References

Antonaglia, J., Xie, X., Schwarz, G., Wraith, M., Qiao, J., Zhang, Y., Liaw, P.K., Uhl, J.T., Dahmen, K.A., 2014. Tuned critical avalanche scaling in bulk metallic glasses. Sci. Rep. 4, 4382.
Bak, P., Tang, C., Wiesenfeld, K., 1987. Self-organized criticality: an explanation of the 1/f noise. Phys. Rev. Lett. 59, 381–384.
Bei, H., Xie, S., George, E.P., 2006. Softening caused by profuse shear banding in a bulk metallic glass. Phys. Rev. Lett. 96, 105503.
Bishop, J.F.W., Hill, R., 1951. XLVI. a theory of the plastic distortion of a polycrystalline aggregate under combined stresses. Phil. Mag. 42, 414–427.
Chen, K.W., Lin, J.F., 2010. Investigation of the relationship between primary and secondary shear bands induced by indentation in bulk metallic glasses. Int. J. Plast. 26, 1645–1658.
Chen, Y., Dai, L.H., 2016. Nature of crack-tip plastic zone in metallic glasses. Int. J. Plast. 77, 54–74.
Cheng, J.L., Chen, G., Xu, F., Du, Y.L., Li, Y.S., Liu, C.T., 2010. Correlation of the microstructure and mechanical properties of Zr-based in-situ bulk metallic glass matrix composites. Intermetallics 18, 2425–2430.
Denisov, D.V., Lorincz, K.A., Uhl, J.T., Dahmen, K.A., Schall, P., 2016. Universality of slip avalanches in flowing granular matter. Nat. Commun. 7, 10641.
Eckert, J., Das, J., Pauly, S., Duhamel, C., 2011. Mechanical properties of bulk metallic glasses and composites. J. Mater. Res. 22, 285–301.
Eshelby, J.D., Frank, F.C., Nabarro, F.R.N., 1951. The equilibrium of linear arrays of dislocations. Phil. Mag. 42, 351–364.
Fornell, J., Concustell, A., Suriñach, S., Li, W.H., Cuadrado, N., Gebert, A., Baró, M.D., Sort, J., 2009. Yielding and intrinsic plasticity of Ti–Zr–Ni–Cu–Be bulk metallic glass. Int. J. Plast. 25, 1540–1559.
Gao, J., Sharp, J., Guan, D., Rainforth, W.M., Todd, I., 2015. New compositional design for creating tough metallic glass composites with excellent work hardening. Acta Mater. 86, 208–215.
Greer, A.L., Cheng, Y.Q., Ma, E., 2013. Shear bands in metallic glasses. Mater. Sci. Eng., R 74, 71–132.
Hansen, N., 2004. Hall–Petch relation and boundary strengthening. Scripta Mater. 51, 801–806.
Hashimoto, K., Margolin, H., 1983. The role of elastic interaction stresses on the onset of slip in polycrystalline alpha brass—I. Experimental determination of operating slip systems and qualitative analysis. Acta Metall. 31, 773–785.
Hofmann, D.C., 2010. Shape memory bulk metallic glass composites. Science 329, 1294–1295.
Hofmann, D.C., Suh, J.Y., Wiest, A., Duan, G., Lind, M.L., Demetriou, M.D., Johnson, W.L., 2008a. Designing metallic glass matrix composites with high toughness and tensile ductility. Nature 451, 1085–1089.
Hofmann, D.C., Suh, J.Y., Wiest, A., Lind, M.L., Demetriou, M.D., Johnson, W.L., 2008b. Development of tough, low-density titanium-based bulk metallic glass matrix composites with tensile ductility. P Natl. Acad. Sci. 105, 0136–20140.
Hufnagel, T.C., Schuh, C.A., Falk, M.L., 2016. Deformation of metallic glasses: recent developments in theory, simulations, and experiments. Acta Mater. 109, 375–393.
Jang, D., Gross, C.T., Greer, J.R., 2010. Effects of size on the strength and deformation mechanism in Zr-based metallic glasses. Int. J. Plast. 27, 858–867.
Jeon, C., Kang, M., Paul Kim, C., Seop Kim, H., Lee, S., 2016. Effects of dendrite size on dynamic tensile deformation behavior in Zr-based amorphous alloys containing ductile dendrites. Mater. Sci. Eng., A 650, 102–109.
Jeon, C., Ha, D.J., Kim, C.P., Lee, S., 2012. Effects of dendrite size on tensile deformation behavior in Zr-Based amorphous matrix composites containing ductile dendrites. Metall. Mater. Trans. A 43, 3663–3674.
Jeon, C., Kang, M., Paul Kim, C., Seop Kim, H., Lee, S., 2013. Quasi-static and dynamic compressive deformation behaviors in Zr-based amorphous alloys containing ductile dendrites. Mater. Sci. Eng., A 579, 77–85.
Jiang, J.Z., Hofmann, D.C., Jarvis, D.J., Fecht, H.J., 2015a. Low-density high-strength bulk metallic glasses and their composites: a review. Adv. Eng. Mater. 17, 761–780.
Jiang, M.Q., Wilde, G., Dai, L.H., 2015b. Origin of stress overshoot in amorphous solids. Mech. Mater. 81, 72–83.
Kolodziejska, J.A., Kozachkov, H., Kranjc, K., Hunter, A., Marquis, E., Johnson, W.L., Flores, K.M., Hofmann, D.C., 2016. Towards an understanding of tensile deformation in Ti-based bulk metallic glass matrix composites with BCC dendrites. Sci. Rep. 6, 22563.
Lee, M.L., Li, Y., Schuh, C.A., 2004. Effect of a controlled volume fraction of dendritic phases on tensile and compressive ductility in La-based metallic glass matrix composites. Acta Mater. 52, 4121–4131.
Lewandowski, J.J., Lowhaphandu, P., 2002. Effects of hydrostatic pressure on the flow and fracture of a bulk amorphous metal. Philos. Mag. A-Phys. Condens. Matter Struct. Defect Mech. Prop. 82, 3427–3441.

Li, X., Wei, Y., Lu, L., Lu, K., Gao, H., 2010. Dislocation nucleation governed softening and maximum strength in nano-twinned metals. Nature 464, 877–880.
Ma, D.Q., Li, J., Zhang, Y.F., Zhang, X.Y., Ma, M.Z., Liu, R.P., 2014. Effect of compositional tailoring on the glass-forming ability and mechanical properties of TiZr-based bulk metallic glass matrix composites. Mater. Sci. Eng., A 612, 310–315.
Meyers, M.A., Mishra, A., Benson, D.J., 2006. Mechanical properties of nanocrystalline materials. Prog. Mater. Sci. 51, 427–556.
Meyersm, M.A., Ashworth, E., 1982. A model for the effect of grain size on the yield stress of metals. Phil. Mag. 46, 737–759.
Nabarro, F.R.N., 1947. Dislocations in a simple cubic lattice. Proc. Phys. Soc., London 59, 256–272.
Narayan, R.L., Boopathy, K., Sen, I., Hofmann, D.C., Ramamurty, U., 2010. On the hardness and elastic modulus of bulk metallic glass matrix composites. Scripta Mater. 63, 768–771.
Nieh, T.G., Nix, W.D., 1986. Unloading yield effects in aluminum alloys. Metall. Trans. A 19A, 121–126.
Oh, Y.S., Paul Kim, C., Lee, S., Kim, N.J., 2011. Microstructure and tensile properties of high-strength high-ductility Ti-based amorphous matrix composites containing ductile dendrites. Acta Mater. 59, 7277–7286.
Qiao, J.C., Yao, Y., Pelletier, J.M., Keer, L.M., 2016b. Understanding of micro-alloying on plasticity in $Cu_{46}Zr_{47-x}Al_7Dy_x$ ($0 \le x \le 8$) bulk metallic glasses under compression: based on mechanical relaxations and theoretical analysis. Int. J. Plast. 82, 62–75.
Qiao, J.W., Sun, A.C., Huang, E.W., Zhang, Y., Liaw, P.K., Chuange, C.P., 2011. Tensile deformation micromechanisms for bulk metallic glass matrix composites: from work-hardening to softening. Acta Mater. 59, 4126–4137.
Qiao, J.W., Jia, H.L., Zhang, Y., Liaw, P.K., Li, L.F., 2012. Multi-step shear banding for bulk metallic glasses at ambient and cryogenic temperatures. Mater. Chem. Phys. 136, 75–79.
Qiao, J.W., Jia, H., Liaw, P.K., 2016a. Metallic glass matrix composites. Mater. Sci. Eng., R 100, 1–69.
Qiao, J.W., Wang, S., Zhang, Y., Liaw, P.K., Chen, G.L., 2009a. Large plasticity and tensile necking of Zr-based bulk-metallic-glass-matrix composites synthesized by the Bridgman solidification. Appl. Phys. Lett. 94, 151905.
Qiao, J.W., Zhang, T., Yang, F.Q., Liaw, P.K., Pauly, S., Xu, B.S., 2013. A tensile deformation model for in-situ dendrite/metallic glass matrix composites. Sci. Rep. 3, 2816.
Qiao, J.W., Zhang, Y., Chen, G.L., 2009b. Fabrication and mechanical characterization of a series of plastic Zr-based bulk metallic glass matrix composites. Mater. Des. 30, 3966–3971.
Qiao, J.W., Zhang, Y., Liaw, P.K., Chen, G.L., 2009c. Micromechanisms of plastic deformation of a dendrite/Zr-based bulk-metallic-glass composite. Scripta Mater. 61, 1087–1090.
Schuh, C.A., Hufnagel, T.C., Ramamurty, U., 2007. Mechanical behavior of amorphous alloys. Acta Mater. 55, 4067–4109.
Song, W., Wu, Y., Wang, H., Liu, X., Chen, H., Guo, Z., Lu, Z., 2016. Microstructural control via copious nucleation manipulated by In Situ Formed Nucleants: Large-sized and Ductile Metallic Glass Composites. Adv. Mater. 28, 8156–8161.
Şopu, D., Stoica, M., Eckert, J., 2015. Deformation behavior of metallic glass composites reinforced with shape memory nanowires studied via molecular dynamics simulations. Appl. Phys. Lett. 106, 211902.
Sun, B.A., Song, K.K., Pauly, S., Gargarella, P., Yi, J., Wang, G., Liu, C.T., Eckert, J., Yang, Y., 2016. Transformation-mediated plasticity in CuZr based metallic glass composites: a quantitative mechanistic understanding. Int. J. Plast. 85, 34–51.
Sun, X.H., Qiao, J.W., Jiao, Z.M., Wang, Z.H., Yang, H.J., Xu, B.S., 2015a. An improved tensile deformation model for in-situ dendrite/metallic glass matrix composites. Sci. Rep. 5, 13964.
Sun, X.H., Wang, Y.S., Fan, J., Yang, H.J., Ma, S.G., Wang, Z.H., Qiao, J.W., 2015b. Plasticity improvement for dendrite/metallic glass matrix composites by pre-deformation. Mater. Des. 86, 266–271.
Swygenhoven, H.V., 2002. Grain boundaries and dislocations. Science 296, 66–67.
Tong, X., Wang, G., Yi, J., Ren, J.L., Pauly, S., Gao, Y.L., Zhai, Q.J., Mattern, N., Dahmen, K.A., Liaw, P.K., Eckert, J., 2016. Shear avalanches in plastic deformation of a metallic glass composite. Int. J. Plast. 77, 141–155.
Wang, G., Chan, K.C., Xia, L., Yu, P., Shen, J., Wang, W.H., 2009. Self-organized intermittent plastic flow in bulk metallic glasses. Acta Mater. 57, 6146–6155.
Wang, S.G., Xu, J., 2013. Strengthening and toughening of Mg-based bulk metallic glass via in-situ formed B2-type AgMg phase. J. Non-Cryst. Solids 379, 40–47.
Wang, W.H., Dong, C., Shek, C.H., 2004. Bulk metallic glasses. Mater. Sci. Eng., R 44, 45–89.
Wang, Y.S., Hao, G.J., Ma, R., Zhang, Y., Lin, J.P., Wang, Z.H., Qiao, J.W., 2015. Quasi-static and dynamic compression behaviors of metallic glass matrix composites. Intermetallics 60, 66–71.
Wu, F.F., Chan, K.C., Jiang, S.S., Chen, S.H., Wang, G., 2014. Bulk metallic glass composite with good tensile ductility, high strength and large elastic strain limit. Sci. Rep. 4, 5302.
Wu, Y., Wang, H., Wu, H.H., Zhang, Z.Y., Hui, X.D., Chen, G.L., Ma, D., Wang, X.L., Lu, Z.P., 2011. Formation of Cu–Zr–Al bulk metallic glass composites with improved tensile properties. Acta Mater. 59, 2928–2936.
Wu, Y., Xiao, Y., Chen, G., Liu, C.T., Lu, Z., 2010. Bulk metallic glass composites with transformation-mediated work-hardening and ductility. Adv. Mater. 22, 2770–2773.
Yang, M.X., Yuan, F.P., Xie, Q.G., Wang, Y.D., Ma, E., Wu, X.L., 2016. Strain hardening in Fe–16Mn–10Al–0.86C–5Ni high specific strength steel. Acta Mater. 109, 213–222.
Yoo, B.G., Kim, J.Y., Kim, Y.J., Choi, I.C., Shim, S., Tsui, T.Y., Bei, H., Ramamurty, U., Jang, J., 2012. Increased time-dependent room temperature plasticity in metallic glass nanopillars and its size-dependency. Int. J. Plast. 37, 108–118.
Zhang, L., Zhang, H., Li, W., Gemming, T., Wang, P., Bönisch, M., Şopu, D., Eckert, J., Pauly, S., 2017a. β-type Ti-based bulk metallic glass composites with tailored structural metastability. J. Alloys Compd. 708, 972–981.
Zhang, L., Zhu, Z., Fu, H., Li, H., Zhang, H., 2017b. Improving plasticity and work-hardening capability of β-type bulk metallic glass composites by destabilizing β phases. Mater. Sci. Eng., A 689, 404–410.
Zhang, T., Ye, H.Y., Shi, J.Y., Yang, H.J., Qiao, J.W., 2014. Dendrite size dependence of tensile plasticity of in situ Ti-based metallic glass matrix composites. J. Alloys Compd. 583, 593–597.
Zhao, P., Li, J., Wang, Y., 2013. Heterogeneously randomized STZ model of metallic glasses: softening and extreme value statistics during deformation. Int. J. Plast. 40, 1–22.
Zhecheva, A., Sha, W., Malinov, S., Long, A., 2005. Enhancing the microstructure and properties of titanium alloys through nitriding and other surface engineering methods. Surf. Coating. Technol. 200, 2192–2207.
Zhou, H., Qu, S., Yang, W., 2013. An atomistic investigation of structural evolution in metallic glass matrix composites. Int. J. Plast. 44, 147–160.
Zhu, Y., Xiang, Y., Schulz, K., 2016. The role of dislocation pile-up in flow stress determination and strain hardening. Scripta Mater. 116, 53–56.